Inorg. Chem. **2003**, *42*, 1467–1474

Laves-Phase Structural Changes in the System $CaAl_{2-x}Mg_x$

Shahrad Amerioun,[†] Sergei I. Simak,[‡] and Ulrich Häussermann*,[†]

Department of Inorganic Chemistry, Stockholm University, 10691 Stockholm, Sweden, and Department of Applied Physics, Chalmers University of Technology and Göteborg University, S-41296 Gothenburg, Sweden

Received October 3, 2002

Compounds $CaAl_{2-x}Mg_x$ ($0 \leq x \leq 2$) were synthesized and structurally characterized by X-ray diffraction experiments. With increasing Mg content x the sequence of Laves phase structures $MgCu_2 \rightarrow MgNi_2 \rightarrow MgZn_2$ is revealed. The homogeneity ranges of the underlying phases were determined to be $0 \leq x < 0.24(1)$ ($MgCu_2$ type), $0.66(2) < x < 1.07(3)$ ($MgNi_2$ type), and $1.51(5) < x \leq 2.0$ ($MgZn_2$ type). Mg/Al site occupancies in $CaAl_{1.34}Mg_{0.66}$ and in $CaAl_{0.44}Mg_{1.56}$ were refined from neutron powder diffraction experiments and exposed a pronounced segregation of Al and Mg in $MgNi_2$-type $CaAl_{1.34}Mg_{0.66}$ where Al atoms preferentially occupy the positions corresponding to trigonal bipyramids. In $MgZn_2$-type $CaAl_{0.44}Mg_{1.56}$, however, the Mg/Al distribution was found to be nearly uniform. Structural stability in the quasi-binary system $CaAl_{2-x}Mg_x$ was investigated by first-principles calculations in which random occupational disorder of Mg and Al was modeled with the virtual crystal approximation. The theoretical calculations reproduced the experimental compositional stability ranges of the three different Laves phase structures very well. Structural changes in the quasi-binary system $CaAl_{2-x}Mg_x$ are induced by the electron concentration, which decreases with increasing x. The stability of the different Laves phase structures as a function of electron concentration was analyzed by the method of moments.

1. Introduction

Laves phases are ubiquitous among intermetallic AB_2 systems. More than 1000 compounds are reported to crystallize in one of the three primary Laves phase structure types $MgCu_2$, $MgZn_2$, or $MgNi_2$.[1] These structures are intimately related and represent close-packed arrangements of differently sized spheres (topological close-packings). It is well-known that for Laves phase AB_2 systems electronic factors—in particular the electron concentration (number of valence electrons/atom)—determine which of the three structure types is adopted. This was already shown by Laves and Witte for the quasi-binary alloys $MgCu_{2-x}X_x$ and $MgZn_{2-x}X_x$ (X = Ag, Al, Si) where distinct homogeneity ranges exist for each type of structure.[2] Johannes and Haydock[3,4] and later Johnston and Hoffmann[5] attempted to establish overall valence electron stability ranges of the three topological close-packings $MgCu_2$, $MgZn_2$, and $MgNi_2$ for transition metal Laves phases. There are also examples of intricated structural stability oscillations induced by rather small changes in the electron concentration. In quasi-binary $MgNi_{2-x}Zn_x$ the structural sequence $MgNi_2 \rightarrow MgCu_2 \rightarrow MgNi_2 \rightarrow MgZn_2$ is realized with increasing x.[6] Additionally, at some stability boundaries of the primary structure types complex stacking variants between them occur. This polytype formation is also observed, for example, in the systems $MgNi_{2-x}Cu_x$, $MgCu_{2-x}Zn_x$, and $MgZn_{2-x}Ag_x$.[6−10]

Although structural competition between the Laves phase structure types $MgCu_2$, $MgZn_2$, and $MgNi_2$ is largely dominated by the electron concentration, a clear structure−

* To whom correspondence should be adddressed. E-mail: ulrich@inorg.su.se.
[†] Stockholm University.
[‡] Chalmers University of Technology and Göteborg University.

(1) Villars, P.; Calvert, L. D. *Pearsons Handbook of Crystallographic Data for Intermetallic Compounds*, 2nd ed.; ASM International: Materials Park, OH, 1991; Desk Edition, 1997.
(2) Laves, F.; Witte, H. *Metallwirtsch., Metallwiss., Metalltech.* **1936**, *15*, 840.
(3) Haydock, R.; Johannes, R. L. *J. Phys. F* **1975**, *5*, 2055.
(4) Johannes, R. L.; Haydock, R.; Heine, V. *Phys. Rev. Lett.* **1976**, *36*, 372.
(5) Johnston, R. L.; Hoffmann, R. *Z. Anorg. Allg. Chem.* **1992**, *616*, 105.
(6) Komura, Y.; Mitarai, M.; Nakaue, A.; Tsujimoto, S. *Acta Crystallogr. B* **1972**, *28*, 976.
(7) Komura, Y.; Nakaue, A.; Mitarai, M. *Acta Crystallogr. B* **1972**, *28*, 727.
(8) Komura, Y.; Mitarai, M.; Nakatani, I.; Iba, H.; Shimizu, T. *Acta Crystallogr. B* **1970**, *26*, 666.
(9) Komura, Y.; Mitarai, M.; Kitano, Y. *Acta Crystallogr. B* **1977**, *33*, 2496.
(10) Komura, Y.; Tokunaga, K. *Acta Crystallogr. B* **1980**, *36*, 1548.

10.1021/ic020596m CCC: $25.00
Published on Web 02/06/2003

Table 1. X-ray Single-Crystal Refinement Data for the Compounds $CaAl_{1.34(2)}Mg_{0.66(2)}$, $CaAl_{0.93(3)}Mg_{1.07(3)}$, $CaAl_{0.44(4)}Mg_{1.56(4)}$, and $CaMg_2$[a]

param	$CaAl_{1.34(2)}Mg_{0.66(2)}$	$CaAl_{0.93(3)}Mg_{1.07(3)}$	$CaAl_{0.44(4)}Mg_{1.56(4)}$	$CaMg_2$
space group	$P6_3/mmc$	$P6_3/mmc$	$P6_3/mmc$	$P6_3/mmc$
fw	92.3	91.2	89.7	88.7
a (Å)	5.8353(4)	5.935(1)	6.0755(4)	6.2613(5)
c (Å)	18.897(3)	19.258(6)	9.7708(7)	10.157(1)
V (Å^3)	557.3(1)	587.5(2)	312.34(4)	344.85(5)
Z	8	8	4	4
ρ_{calcd} (g/cm^3)	2.24	2.05	1.89	1.70
μ (mm^{-1})	2.45	2.28	2.10	1.88
R_1	0.0284	0.0184	0.030	0.011
wR_2	0.0406	0.0318	0.099	0.024

[a] The listed composition of the ternaries were obtained from EDX analyses and the lattice parameters from X-ray powder data. $R_1 = \sum|F_o| - |F_c|/\sum|F_o|$. $wR_2 = (\sum[w(F_o^2 - F_c^2)^2])/(\sum[w(F_o^2)^2])$, with $w = 1/[\sigma^2(F_o^2) + (aP)^2 + bP]$ and $P = (F_o^2 + 2F_c^2)/3$.

electron count relationship is obscured for two reasons: (i) The possibility of the A and B component having different electronegativities gives rise to varying ratios of A- and B-based states in the occupied AB_2 bands. (ii) Laves phases form in principle between metallic elements from all parts of the periodic table. Therefore the A-*l* and B-*l* orbital nature of the occupied bands may be changed when comparing different chemical systems displaying Laves phases and structural trends may alter. For example, in the system $MgCu_{2-x}Zn_x$ the sequence of primary Laves phase structure types $MgCu_2 \rightarrow MgNi_2 \rightarrow MgZn_2$ is observed for increasing x,[6,8] i.e., increasing electron concentration, whereas in $CaAl_{2-x}Li_x$ the same sequence is realized for *decreasing* electron concentration.[11]

In this work we investigate in detail structural stability of the main group Laves phases in quasi-binary $CaAl_{2-x}Mg_x$. Electron concentration controlled sequences of Laves phase structures among main group intermetallic systems are hitherto only known for $CaAl_{2-x}Li_x$.[11] In particular, we established the homogeneity ranges of the different structure types in the system $CaAl_{2-x}Mg_x$ and additionally investigated Al/Mg ordering tendencies. The experimental results are compared with first-principles electronic structure calculations, and the electron concentration induced structural sequence in $CaAl_{2-x}Mg_x$ is interpreted with the simple and chemically transparent method of moments.

2. Experimental Section

2.1. Synthesis and Compositional Analysis. The binary compounds $CaAl_2$ and $CaMg_2$ were prepared from the elements and handled in an Ar-filled glovebox (O_2 concentration < 10 ppm). The pure elements, Ca granulates (ABCR, 99.9%), Mg granulates (ABCR, 99.9%), and Al ingots (Aldrich, 99.9%), were weighed in Ta ampules, which were sealed and placed in fused silica Schlenk tubes under reduced pressure. Reactant mixtures were heated to 800−850 °C for 24 h to ensure complete melting followed by rapid quenching to room temperature and subsequent annealing at 700 °C for 5 days. Compounds $CaAl_{2-x}Mg_x$ (nominal compositions x = 0.33, 0.67, 0.75, 1.0, 1.25, 1.33, 1.5, 1.67) were prepared by heating stoichiomteric amounts of $CaAl_2$ and $CaMg_2$ to 700 °C for 10 days, followed by slowly cooling at a rate of 20 °C/h to room temperature. All products, which were highly crystalline and exhibited a silvery-gray metallic luster, were characterized by Guinier powder diagrams (Cu Kα; Si standard). The composition of the products was analyzed with the EDX (energy-disperse X-ray) method in a JEOL 820 scanning electron microscope averaging at least 10 analyses for each sample. EDX analyses revealed a loss of Mg in the ternary products (up to 10 at. %). The limiting compositions of the structure types $MgCu_2$, $MgNi_2$, and $MgZn_2$ were determined from the samples $x = 0.67$ and $x = 1.5$ which represented two-phase regions of $MgCu_2/MgNi_2$ and $MgNi_2/MgZn_2$, respectively.

2.2. Structure Determination. X-ray Investigations. The lattice constants of the investigated $CaAl_{2-x}Mg_x$ system were obtained from least-squares refinement of measured and indexed lines of the corresponding Guinier powder diffractograms.[12] To ensure proper assignment of the indices the observed lines were compared with the calculated ones[13] using the positional parameters resulting from the structure refinements. Single-crystal intensity data were collected at 293 K from at least two different crystals from each of the samples $CaAl_{1.34}Mg_{0.66}$, $CaAl_{1.07}Mg_{0.93}$, $CaAl_{0.44}Mg_{1.56}$ (EDX-determined compositions), and $CaMg_2$ on a STOE IPDS diffractometer with monochromatic Mo Kα radiation (λ = 0.710 73 Å). The sample compositions corresponded to the homogeneity range borders of the $MgNi_2$ and $MgZn_2$ structure types, respectively. All data sets were corrected for Lorentz and polarizations effects. Absorption correction was performed by the program X-shape as included in the STOE IPDS software.[14] For structure refinement (full-matrix least squares on F^2) the program SHELXL97[15] was used. The structures were refined using the atomic position parameters of the $MgNi_2$ and $MgZn_2$ structures (space group $P6_3/mmc$) as a starting model. Some details of the single-crystal data collections and refinements are listed in Table 1. Atomic position parameters and selected interatomic distances are given in Tables 3 and 4. Further details of the crystal structure investigation may be obtained as Supporting Information.

Neutron Investigations. X-ray diffraction studies are unable to discriminate between Mg (Z = 12) and Al (Z = 13) whereas the neutron scattering lengths of those elements differ by about 35%. Neutron diffraction experiments on $CaAl_{1.34(2)}Mg_{0.66(2)}$ and $CaAl_{0.44(4)}Mg_{1.56(4)}$ (EDX-determined compositions) obtained from the samples with nominal composition $CaAl_{1.25}Mg_{0.75}$ and $CaAl_{0.33}Mg_{1.67}$, respectively, were performed on the Polaris powder diffractometer at the ISIS facility, Chilton, U.K., with the samples encapsulated inside thin-walled vanadium cans. Time-of-flight diffraction data were collected at room temperature using the backscattering detector bank which covers the scattering angles 135° < ±2θ < 160° and

(11) Nesper, R.; Miller, G. J. *J. Alloys Compds.* **1993**, *197*, 109.
(12) Werner, P.-E. *Ark. Kemi* **1969**, *31*, 513.
(13) Yvon, K.; Jeitschko, W.; Parthé, E. *J. Appl. Crystallogr.* **1977**, *10*, 73.
(14) *IPDS*, version 2.87; Stoe and Cie GmbH: Darmstadt, Germany, 1996. *XSHAPE*: *Crystal Optimisation for Numerical Absorption Correction*; Stoe and Cie GmbH: Darmstadt, Germany, 1996.
(15) Sheldrick, G. M. *SHELXL97*; University of Göttingen, Göttingen, Germany, 1997.

Table 2. Structural Parameters of the Laves Phase Structure Types

structure	atom	site	coordinates	idealized
$MgCu_2$	A	8a	1/8, 1/8, 1/8	
$Fd\bar{3}m$	B	16d	1/2, 1/2, 1/2	
$MgZn_2$	A	4f	1/3, 2/3, *z*	$z = 1/16 = 0.0625$
$P6_3/mmc$	B1	2a	0, 0, 0	
	B2	6h	*x*, 2*x*, 1/4	$x = 5/6 = 0.8333$
				$c/a = \sqrt{8/3} = 1.633$
$MgNi_2$	A1	4e	0, 0, *z*	$z = 3/32 = 0.09375$
$P6_3/mmc$	A2	4f	1/3, 2/3, *z*	$z = 27/32 = 0.84375$
	B1	4f	1/3, 2/3, *z*	$z = 1/8 = 0.125$
	B2	6h	*x*, 2*x*, 1/4	$x = 1/6 = 0.16667$
	B3	6g	0, 1/2, 1/2	
				$c/a = 4\sqrt{2/3} = 3.26$

provides data over the *d*-spacing range $0.5 < d < 3.2$ Å with a resolution $\Delta d d^{-1} = 5 \times 10^{-3}$. Rietveld profile refinements using the normalized diffraction data were performed using the program FULLPROF.[16] The samples were found to contain small amounts of pure Mg (which confirms the loss of Mg observed by EDX) and CaO. A multiphase refinement was performed including four background parameters and three profile parameters for each phase. Additionally, an absorption correction parameter was employed for the ternary phase. The refined weight fractions were as follows: $CaAl_{1.34(2)}Mg_{0.66(2)}$, 91(4)%; CaO, 4.0(2)%; Mg, 4.8(2)%; $CaAl_{0.44(4)}Mg_{1.56(4)}$, 92(3)%; CaO, 6.4(2)%; Mg, 1.5(2)%. Initial values for the atomic coordinates for each Laves phase were obtained from the single-crystal X-ray diffraction experiments. The B atom sites of the Laves phases were refined for partial Al/Mg occupancy. Due to the rather large correlation between temperature factors and occupancies, the total Al/Mg ratio was constrained to the value obtained from EDX analyses. A number of 31 and 23 parameters were refined for $CaAl_{1.34(2)}Mg_{0.66(2)}$ ($R_p = 0.034$, $R_{wp} = 0.029$, $R_{Bragg} = 0.045$) and $CaAl_{0.44(4)}Mg_{1.56(4)}$ ($R_p = 0.035$, $R_{wp} = 0.032$, $R_{Bragg} = 0.022$), respectively. The results of the Rietveld analyses are presented in Table 3, together with those of the X-ray investigations.

2.3. Electronic Structure Calculations. The $CaAl_{2-x}Mg_x$ system was studied in the framework of the frozen core all-electron projected augmented wave (PAW) method[17] (as implemented in the program VASP[18]). The energy cutoff was set to 240.4 eV. Exchange and correlation effects were treated by the generalized gradient approximation (GGA),[19] usually referred to as PW91. The integration over the Brillouin zone was done on special *k*-points determined according to the Monkhorst−Pack scheme.[20] All necessary convergence tests were performed, and generally the required total energy convergence (within 1.5 meV/atom) was reached for 15 to 60 *k*-points in the irreducible wedge of the Brillouin zone depending on the structure and total number of atoms. Al/Mg disorder was taken into account within the so-called virtual-crystal approximation (VCA) which is the simplest approximation in the hierarchy of mean-field approaches.[21,22] Positions on the sublattices occupied randomly by Al or Mg were treated as a fictitious atoms with the nuclear charge $Z = xZ_{Al} + (1 - x)Z_{Mg}$ (where Z_X is the corresponding nuclear charge of the pure element X) and a corresponding number of valence electrons as to force charge neutrality. The mean-field treatment is sufficient to describe the case of randomly distributed atoms,[21−23] and in particular it has been shown that VCA is a suitable approximation for calculating the electronic structure of alloys between neighboring elements in the periodic table.[24]

3. Results and Discussion

Laves phases AB_2 occur in three primary structure types, namely cubic $MgCu_2$ (space group $Fd\bar{3}m$) and hexagonal $MgZn_2$ and $MgNi_2$ (space group $P6_3/mmc$). The close relationship between these structures becomes especially apparent when $MgCu_2$ is defined rhombohedrally with hexagonal axes of reference. In $MgCu_2$ (Figure 1a) B atoms form a network of vertex condensed tetrahedra. The arrangement of the A atoms corresponds to that of (cubic) diamond. In $MgZn_2$ (Figure 1b) the B atom network consists of trigonal bipyramids which are condensed via the two apex atoms along the *c* direction. The chains are linked by connecting the vertexes in the *ab* plane. The A atom structure in $MgZn_2$ corresponds to that of hexagonal diamond. Finally, the $MgNi_2$ structure (Figure 1c) represents a 1:1 composite of the $MgCu_2$ and $MgZn_2$ structures. The B atom networks in the Laves phase structure types can also be described as stackings of Kagomé (3636) and 3^6 nets. The former are three times as dense as the latter. Importantly, in all three structure types A and B atoms possess the same number of nearest neighbors.[25,26] The structural parameters of the Laves phase structure types are compiled in Table 2.

The cubic $MgCu_2$ structure, where A and B atoms occupy the high-symmetry sites 8a and 16d, does not possess any structural flexibility. In $MgZn_2$ the B atom network consists of two different kind of atoms, B1 and B2. The Kagomé net making up the triangular waists of the B_5 trigonal bipyramids is defined by the 6h site (B2 atoms). The triangle capping atoms (3^6 net), which are shared between two trigonal bipyramids, correspond to the B1 atoms (site 2a). The free parameter *x* of the site 6h allows the Kagomé net to distort as indicated in Figure 1d. In the $MgZn_2$ structure there are three different distances within the B framework, B_{12}, $B_{22}{}^c$, and $B_{22}{}^u$ (cf. Figure 1d) and two different distances A−B. In the $MgNi_2$ structure the B atom network is composed of three different atoms B1, B2, and B3 which occupy the sites 4f, 6h, and 6g, respectively. The sites 6h (B2 atoms) and 6g (B3 atoms) define a flexible and a rigid Kagomé net, respectively. The B1 atoms on 4f form the triangle-capping 3^6 net which completes the B atom framework of vertex condensed tetrahedra and trigonal bipyramids of $MgNi_2$. In the $MgNi_2$ structure there are now five different distances within the B framework, B_{12}, $B_{22}{}^c$, $B_{22}{}^u$, B_{13}, and B_{33}, and four different distances A−B. For the hexagonal structures a set of parameters can be specified which yields idealized

(16) Rodriguez-Carvajal, J. *FULLPROF: Program for Rietveld Analysis of Neutron and X-ray Powder Diffraction Data*, version 2k; Laboratoire Leon Brillouin: CEA-Saclay: Saclay, France, 2000.
(17) Blöchl, P. E. *Phys. Rev. B* **1994**, *50*, 17953. Kresse, G.; Joubert, J. *Phys. Rev. B* **1999**, *59*, 1758.
(18) Kresse, G.; Hafner, J. *Phys. Rev. B* **1993**, *47*, RC558. Kresse, G.; Furthmüller, J. *Phys. Rev. B* **1996**, *54*, 11169.
(19) Perdew, J. P.; Wang, Y. *Phys. Rev. B* **1992**, *45*, 13244.
(20) Monkhorst, H. J.; Pack, J. D. *Phys. Rev. B* **1972**, *13*, 5188.
(21) Faulkner, J. S. *Prog. Mater. Sci.* **1982**, *27*, 3.
(22) Ducastelle F. *Order and Phase Stability in Alloys*; North-Holland: Amsterdam, 1991.
(23) Abrikosov, I. A.; Johansson, B. *Phys. Rev. B* **1998**, *57*, 14164.
(24) Abrikosov, I. A.; James, P.; Eriksson, O.; Söderlind, P.; Ruban, A. V.; Skriver, H. L.; Johansson, B. *Phys. Rev. B* **1996**, *54*, 3380.
(25) Hyde, B. G.; Andersson, S. *Inorganic Crystal Structures*; John Wiley & Sons: New York, 1989.
(26) Müller, U. *Inorganic Structural Chemistry*; John Wiley & Sons: Chichester, U.K., 1993.

Table 3. Atomic Position Parameters, Site Occupancies, and Isotropic Thermal Displacement Parameters (Å^2) for $CaAl_{2-x}Mg_x$[a]

x for $CaAl_{2-x}Mg_x$	param	Ca1	Ca2	B1	B2	B3
$x = 0.66$	ref posn	0.09404(6)	0.84304(6)	012941(8)	0.1629(2)	
		0.0939(1)	*0.8428(1)*	*0.1291(2)*	*0.1631(6)*	
	U_{eq}	0.0110(3)	0.0100(2)	0.0126(3)	0.0113(3)	0.0067(3)
		0.011(8)	*0.0117(8)*	*0.013(1)*	*0.015(1)*	*0.019(1)*
	sof	1	1	*0.28(2) (Mg)*	*0.19(1) (Mg)*	*0.50(2) (Mg)*
$x = 1.07$	ref posn	0.0944(5)	0.84313(5)	0.12854(7)	0.1634(3)	
	U_{eq}	0.0120(3)	0.0116(3)	0.0149(3)	0.0076(3)	0.0159(3)
$x = 1.56$	ref posn	0.0617(2)		0.8311(4)		
		0.0623(1)		*0.8312(2)*		
	U_{eq}	0.0166(1)	0.014(1)	0.0212(8)		
		0.0171(6)	*0.0183(8)*	*0.0165(5)*		
	sof	1	*0.72(2) (Mg)*	*0.80(1) (Mg)*		
$x = 2.0$	ref posn	0.06190(3)		0.83129(4)		
	U_{eq}	0.0151(1)	0.0152(2)	0.0150(1)		

[a] Values in italics are results from Rietveld refinements of neutron diffraction powder data. U_{eq} is defined as one-third of the trace of the orthogonalized $\mathbf{U}_{ij}$ tensor.

Table 4. Distances (Å) within the B Atom Framework of the Laves Phases $CaAl_{2-x}Mg_x$[a]

x for $CaAl_{2-x}Mg_x$	B_{22}^c	B_{22}^u	B_{12}^c	B_{13}^c	B_{33}^c
0	2.841				
0.14	2.860				
0.24	2.863				
0.66	2.982(3)	2.854(3)	2.856(2)	2.970	2.918(2)
0.73	3.008(3)	2.880(3)	2.884(2)	2.998	2.944
1.07	3.027(3)	2.909(3)	2.920(2)	3.011	2.968
1.51	3.078(2)	2.992(2)	3.020		
1.56	3.077(7)	2.998(7)	3.021(2)		
1.86	3.124(2)	3.057(2)	3.083		
2.0	3.169	3.092	3.129		

[a] Notation of distances is according to Figure 1d. Only standard deviations larger than 0.001 Å are given.

structures with all distances A−A, A−B, and B−B equal. These parameters for $MgZn_2$ and $MgNi_2$ are also given in Table 2.

The main group intermetallic compounds $CaAl_2$ and $CaMg_2$ crystallize with the $MgCu_2$ and $MgZn_2$ structures, respectively.[27,28] In the quasi-binary system $CaAl_{2-x}Mg_x$ Al and Mg atoms together form the Laves phase B atom framework. This system reveals additionally the $MgNi_2$ structure type stable in a compositional range of $0.66(2) < x < 1.07(3)$. $CaAl_{2-x}Mg_x$ is only the second main group intermetallic system which adopts the $MgNi_2$ structure. We found the $MgNi_2$ stability range separated by two-phase regions from that of the $MgCu_2$ type at low Mg concentrations x ($0 \le x < 0.24(1)$) and that of the $MgZn_2$ type at high Mg concentration x ($1.51(5) < x \le 2$). Figure 2 summarizes homogeneity ranges as well as volumes and lattice parameters of the different phases as a function of x. The variation of the lattice parameters corresponds roughly to Vegard's rule, which states that solid solution lattice parameters vary linearly with composition. This behavior is usually observed in quasi-binary Laves phase systems, despite the occurring structural transitions.[29] The c/a ratios and atomic position parameters of the hexagonal phases deviate only slightly from the values of the idealized structure (cf. Tables 1 and 3).

An important question is the distribution of Mg and Al atoms on the different sites of the B atom framework in the hexagonal structures. Our Rietveld refinement of neutron powder diffraction data for $CaAl_{1.34}Mg_{0.66}$ exhibited an interesting result. $CaAl_{1.34}Mg_{0.66}$ is located at the homogeneity range border of the $MgNi_2$ structure toward lower Mg concentrations. We found that Al occupies preferentially the site 6h corresponding to the flexible Kagomé net (distribution 81% Al/19% Mg). Also the site 4f, which caps the Kagomé nets, shows a tendency of preferred Al occupation (72% Al) with respect to the average concentration 67% Al/33% Mg as given by the composition. The site 6g corresponding to the rigid Kagomé net is occupied by a 50% mixture of Mg and Al. The partial segregation of Al into the positions of the trigonal bipyramids in $MgNi_2$-type $CaAl_{1.34}Mg_{0.66}$ is supported by the distribution of interatomic distances in the B atom framework. The shortest distances of 2.85 and 2.86 Å (B_{22}^u and B_{12}, respectively) occur within layers of trigonal bipyramids, whereas the distances within the tetrahedral part of the $MgNi_2$ type B atom framework (i.e. the distances B_{33} and B_{13}) are considerably larger (Table 4). The short distances in the bipyramidal layers coincide with the B−B distance within the tetrahedral framework of $MgCu_2$-type $CaAl_{1.76}Mg_{0.24}$, which is 2.86 Å. For this compound the Mg concentration on the B atom site (24% Mg) corresponds almost to the average Mg concentration on the sites of the trigonal bipyramids in $MgNi_2$-type $CaAl_{1.34}Mg_{0.66}$ (22% Mg). In contrast to $CaAl_{1.34}Mg_{0.66}$ the Mg/Al site distribution in $MgZn_2$-type $CaAl_{0.44}Mg_{1.54}$ is nearly uniform. However, the latter finding is not in contradiction with the fact that Al has a general tendency to segregate into sites defining trigonal bipyramidal entities. The formation of deltahedral cluster arrangements is a frequent phenomenon in the structural chemistry of polar intermetallics involving group 13 elements. Compared to the other group 13 elements the clustering tendency of Al is least pronounced, but there are several examples of trigonal bipyramidal clusters formed by Al (e.g., in the structures of the compounds Ba_3Al_5, Ba_4Al_5, Ba_7Al_{13}, and Sr_5Al_9[30−33]).

(27) Iandelli, A.; Palenzona, A. *J. Less-Common Met.* **1972**, *29*, 293.
(28) Novotny, H. *Z. Metallkd.* **1946**, *37*, 31.
(29) Simon, A. *Angew. Chem., Int. Ed. Engl.* **1983**, *22*, 97.
(30) Fornasini, M. L. *Acta Crystallogr. C* **1988**, *44*, 1355.
(31) Fornasini, M. L. *Acta Crystallogr. B* **1975**, *31*, 2551.

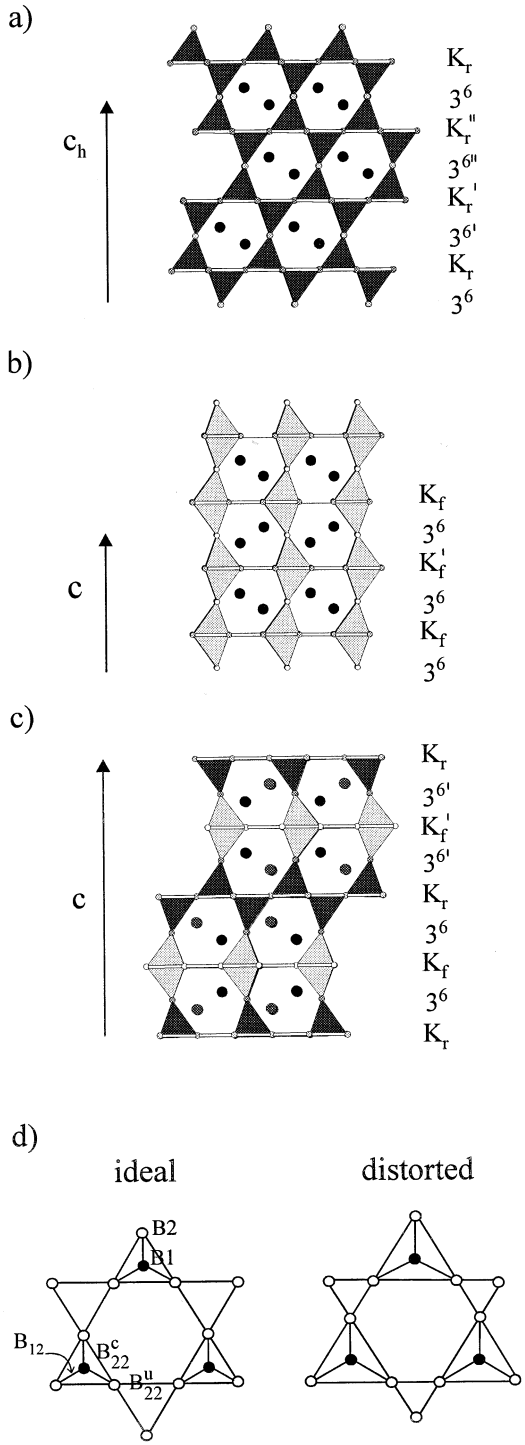

Figure 1. Laves phase AB_2 structure types $MgCu_2$ (defined with respect to a hexagonal unit cell) (a), $MgZn_2$ (b), and $MgNi_2$ (c) projected along the [110] direction. This view emphasizes the connectivity of B_4 tetrahedra and B_5 trigonal bipyramids. The small circles denote B atoms; large circles denote A atoms. The B atom framework may also be described as alternate stacking of 3^6 and Kagomé nets along the *c* direction. This is indicated at the right-hand side of the figures where K_r and K_f distinguish a rigid and flexible Kagomé net, respectively. (d) Distortion of the flexible Kagomé net defined by the Wyckoff site 6h in $MgZn_2$ and $MgNi_2$. The denotion of the distances is adapted from ref 5.

Figure 3 displays the structural energy of the different Laves phase structures in the system $CaAl_{2-x}Mg_x$ as a function of the Mg concentration. The structural energy curves represent the computed total energy differences with

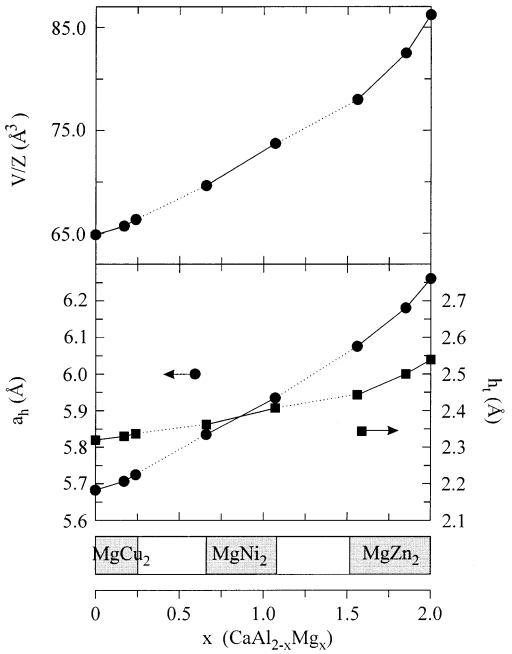

Figure 2. Volumes and lattice parameters for the system $CaAl_{2-x}Mg_x$ as a function of composition. h_t is the (average) thickness of a tetrahedral layer. $h_t = {}^1/_6 c_{h,MgCu_2} = {}^1/_4 c_{MgZn_2} = {}^1/_8 c_{MgNi_2}$. The homogeneity ranges are marked at the bottom.

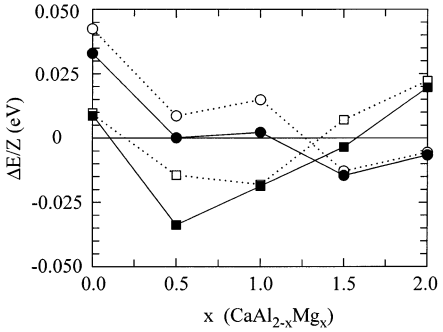

Figure 3. Total energy differences as a function of composition for the system $CaAl_{2-x}Mg_x$ in the $MgZn_2$ (circles), $MgNi_2$ (squares), and $MgCu_2$ structures. The latter represents the reference. Solid and open symbols refer to completely relaxed and idealized hexagonal structures, respectively.

respect to the cubic $MgCu_2$ structure. For each composition $x = 0$, 0.5, 1.0, 1.5, and 2.0 we performed two sets of calculations. In the first set we completely relaxed the three structure types with respect to volume, *c*/*a* ratio, and atomic positional parameters. In the second set we considered the hexagonal structures as ideal (cf. Table 2) with all distances A−A, A−B, and B−B equal and only performed a volume relaxation. The theoretical calculations mirror excellently the experimentally determined homogeneity ranges of the Laves phase type structures. In particular we obtain for $x = 0$ the $MgCu_2$ structure, for $x = 0.5$ and 1.0 the $MgNi_2$ structure, and for $x = 1.5$ and 2.0 the $MgZn_2$ structure lowest in energy. Importantly, this result is also obtained when considering the hexagonal structures as ideal. Thus, neither the possibility of different Al/Mg distributions on the B atom sites (note

(32) Fornasini, M. L.; Bruzzone, G. *J. Less-Common Met.* **1975**, *40*, 335.
(33) Manyako, N. B.; Zarechnyuk, O. S.; Yanson, T. I. *Sov. Phys. Crystallogr.* **1987**, *32*, 196.

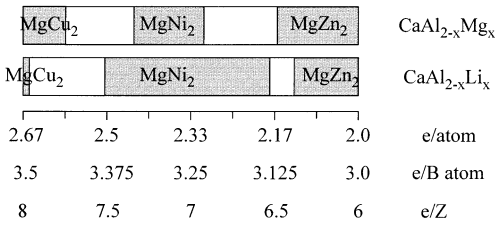

Figure 4. Electron concentration stability ranges of Laves phase structure series in the systems $CaAl_{2-x}Mg_x$ and $CaAl_{2-x}Li_x$.

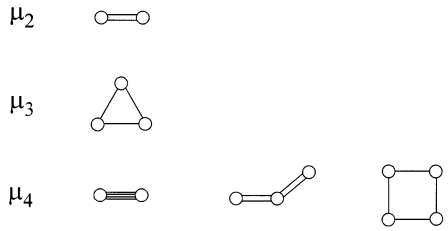

Figure 5. Contributions of local atomic arrangements to the second to fourth moments. Each line represents all possible resonance integrals H_{ij} between two atoms.

that our calculations are based on a complete random distribution of Al and Mg atoms) nor the possibility of a structural distortion decisively influence structural stability in the system $CaAl_{2-x}Mg_x$. As a consequence, we can unambiguously attribute the structural changes to variations in the electron concentration.

The regions between the experimental homogeneity ranges of the different Laves phase coincide with those areas in the structural energy plot where the total energy difference between the different structure types becomes small. In the regions between the compositional stability ranges of two different $CaAl_{2-x}Mg_x$ Laves phases we observed a macroscopic mixture of phases with the corresponding boundary compositions (two-phase regions). This is in contrast to systems such as $MgNi_{2-x}Cu_x$, $MgCu_{2-x}Zn_x$, or $MgZn_{2-x}Ag_x$, where between the stability ranges of the primary Laves phase structure types the formation of complex polytypes—i.e., the formation of microscopic mixtures of the primary structure types—occur.[6−10] We performed TEM investigations on various crystals of samples from two-phase regions but could not detect any indication of such a polytype formation in $CaAl_{2-x}Mg_x$.

Our results for $CaAl_{2-x}Mg_x$ are very similar to the those obtained by Miller and Nesper for the system $CaAl_{2-x}Li_x$.[11] For the latter system variation in the Li:Al ratio allows changes in the electron concentration. In Figure 4 we compare the electron concentration stability ranges of the Laves phase structure types for these two systems. The main difference is the larger domain of structural stability of the $MgNi_2$ type in $CaAl_{2-x}Li_x$. Interestingly, in $CaAl_{2-x}Li_x$ a two-phase region extends from CaAlLi to $CaLi_2$ with both border compositions adopting the $MgZn_2$ structure. The similar domains of structural stability in $CaAl_{2-x}Mg_x$ and $CaAl_{2-x}Li_x$ strongly supports that as for transition metal Laves phases also for purely s−p-bonded main group intermetallic systems the electron concentration determines which of the three Laves phase structures is realized. The examination of the $CaAl_{2-x}Mg_x$ band structures (not shown) reveals that the occupied bands are predominately composed of Al/Mg states. This situation reminds of polar intermetallic compounds which are composed of an oxidized electropositive component and a polyanionic (reduced) network or cluster arrangement. Thus, it can be assumed that in $CaAl_{2-x}Mg_x$ a substantial charge transfer takes place from the Ca atoms to the B atom framework. This suggests to explain the origin of the structural sequence in $CaAl_{2-x}Mg_x$ (and $CaAl_{2-x}Li_x$) stability trends by just considering electronic structure changes in the B atom substructure. For that purpose we will employ the method of moments in the framework of TB (Hückel) theory.

The definition of the *n*th moment of a density of states is $\mu_n = \int_{-\infty}^{\infty} \epsilon^n \, \mathrm{DOS}(\epsilon) \, \mathrm{d}\epsilon$, where ϵ's are the one-electron states and $\mathrm{DOS}(\epsilon)$ is the density of states per atom of the system.[34−36] Considering the relative stability of two structures as a function of electron concentration (i.e. their structural energy), then the first few disparitive moments control the oscillatory behavior of the energy curve. Alternatively, the *n*th moment is given by the sum over different paths all starting off orbital *i* and returning in *n* steps back to this orbital, each step being weighted with the appropriate resonance integral H_{ij}. This has a powerful meaning when expressing the moments with respect to different sites rather to orbitals. The first moment represents only the atom (summation over the Coulomb integrals), the second moment includes together with the third moment the nearest-neighbor interactions, and the forth moment also carries information about the second nearest-neighbor interactions, etc. μ_0 is normalized to 1. In the order from the first to higher moments step by step, information about interactions between a center and its environment at an increasing distance from it is successively achieved. In Figure 5 the contributions of local atomic arrangements to the first few moments are collected. It is easily seen that bond angles and *n*-membered rings generate the most decisive contributions to a particular moment. Thus, the method of moments allows one to put down the relative stability of two structures to differences in local structural features such as different numbers of *n*-membered rings and differences in bond angles.[37−40]

We now apply these ideas to the B atom networks of the Laves phase structures. Let us consider that the networks (i) are ideal, (ii) have the same density, and (iii) are composed of only one and the same kind of (sp) metal atom. Then the first three moments become identical: $\Delta\mu_1 = 0$ because the networks are built up by the same kind of atoms, $\Delta\mu_2 = 0$ because in all networks the B atoms have the same number of nearest neighbors (6) at the same distance, and $\Delta\mu_3 = 0$ because in all networks the number of (equilateral) triangles

(34) Ducastelle, F.; Cyrot-Lackmann, F. *J. Phys. Chem. Solids* **1971**, *32*, 285.
(35) Pettifor, D. G. *Bonding and Structure of Molecules and Solids*; Clarendon Press: Oxford, U.K., 1995.
(36) Burdett, J. K.; Lee, S. *J. Am. Chem. Soc.* **1985**, *107*, 3050.
(37) Burdett, J. K.; Lee, S. *J. Am. Chem. Soc.* **1985**, *107*, 3063.
(38) Lee, S. *Acc. Chem. Res.* **1991**, *21*, 189.
(39) Cressoni, J. C.; Pettifor, D. G. *J. Phys.: Condens. Matter* **1991**, *3*, 495.
(40) Häussermann, U.; Nesper, R. *J. Alloys Compds.* **1995**, *218*, 244.

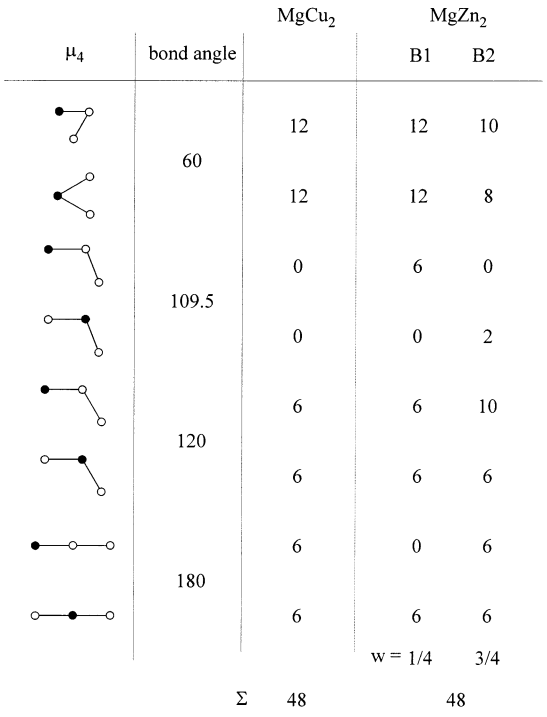

Figure 6. Comparison of the three-atom fourth moment contributions in cubic $MgCu_2$ and hexagonal $MgZn_2$. The solid atom indicates the site from which the path starts and to which it eventually returns. For the $MgZn_2$ structure the B1 and B2 atoms have different weights according to $AB1_{0.5}$-$B2_{1.5}$.

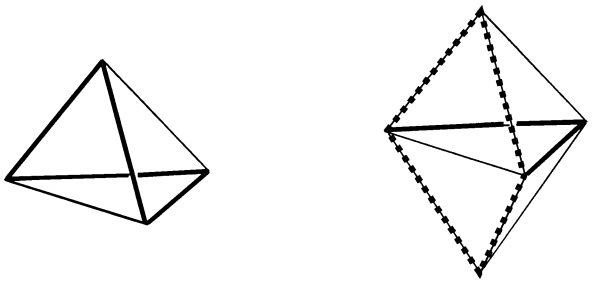

Figure 7. Four-membered ring fourth moment contributions (indicated by thick solid and broken lines) in a tetrahedron and a trigonal bipyramid.

connected to each B atom is the same (6). Thus, the first disparitive moment will be the fourth moment and the structural energy curves will have at least four nodes. In Figure 6 we specify the three-atom fourth moment contributions in the $MgCu_2$ and $MgZn_2$ structure and count them with respect to one B atom. Both structures have in total the same number of three-atom paths describing bond angle contributions. However, their distribution over the occurring framework bond angles 60, 109.5, 120, and 180° is different. If we assume that the three-atom fourth moment contributions are only weakly dependent on the bond angle in the range between 60 and 180°, the four-membered ring contributions will be responsible for the fourth moment disparity of $MgCu_2$ and $MgZn_2$. In this case the $MgZn_2$ structure has a higher fourth moment than the $MgCu_2$ structure. This is due to the occurrence of additional four-membered rings which only are connected to trigonal bipyramids (shown in Figure 7).

The higher fourth moment stabilizes the $MgZn_2$ structure at lower electron concentrations (lower band filling) with respect to the $MgCu_2$ structure.[35,36] This is in agreement with the experimental findings and the results from the first-principles calculations. We can, therefore, understand the origin of the structural trends in $CaAl_{2-x}Mg_x$ and $CaAl_{2-x}Li_x$ from $MgCu_2 \rightarrow MgNi_2 \rightarrow MgZn_2$ with decreasing electron concentration by a successive increase of the four-membered ring concentration in the B atom networks of the Laves phase structure types in this sequence. However, we should note that in our estimation of the fourth moment of the $MgCu_2$ and $MgZn_2$ structures we neglected the angular dependence of the three-atom fourth moment contribution. In reality this contribution is an involved function of the mixing of s and p valence orbitals. Only for the pure s case there is no bond-angle dependence; for the pure p case a pronounced minimum occurs at 90°.[35,39] For the general case of s−p mixing this minimum becomes much less marked and shifts to higher angles. The degree of s−p mixing, which is largely determined by the energetic separation of the s and p valence orbitals, thus highly influences the fourth moment. Therefore, depending on the kind of (sp) metal B atoms, the three-atom fourth moment contribution in the $MgCu_2$ structure may outweigh the fewer number of four-membered rings compared to the $MgZn_2$ structure and differences in the next higher, i.e., the fifth or even sixth, moment will control the structural energy curve.

4. Conclusions

This study reports on Laves phase AB_2 structural changes in the quasi-binary system $CaAl_{2-x}Mg_x$. The cubic $MgCu_2$ structure of binary $CaAl_2$ is stable until the composition $CaAl_{1.76(1)}Mg_{0.24(1)}$ is reached. The hexagonal $MgZn_2$ structure of $CaMg_2$ has a border composition of $CaAl_{0.49(5)}Mg_{1.51(5)}$. In the compositional range of $0.66(2) < x < 1.07(3)$, $CaAl_{2-x}Mg_x$ adopts the $MgNi_2$ structure which represents a 1:1 composite of the $MgCu_2$ and $MgZn_2$ structure type. Neutron diffraction experiments were used to extract the site distribution of Al and Mg atoms in the B atom networks of the hexagonal $MgNi_2$ and $MgZn_2$ structures. It was found that Al and Mg atoms partially segregate in the $MgNi_2$ structure but show a nearly uniform distribution in the $MgZn_2$ structure. $CaAl_{2-x}Mg_x$ is the second main group intermetallic system which displays the $MgNi_2$ Laves phase structure and thus corroborates that electron concentration controlled sequences of Laves phase structures also occur among main group intermetallics.

First-principles calculations reproduced excellently the experimentally obtained structural sequence $MgCu_2 \rightarrow MgNi_2 \rightarrow MgZn_2$ as a function of the electron concentration. The origin of this structural trend was explained by fourth moment differences in the density of states of the three Laves phase structure types. The successive increase of the number of four-membered rings in the B atom networks increases the fourth moment in the direction $MgCu_2 \rightarrow MgNi_2 \rightarrow MgZn_2$, and the structural sequence is realized for decreasing electron concentration. This simple and quite attractive explanation is based on the assumption that in main group Laves phase systems the occupied bands are dominated by B atom states and structural stability trends can be discussed

by only considering B atom interactions. This approximation is not justified for Laves phases containing transition metals, where in general smaller electronegativity differences between the A and B component occur. When A atom bonding contributions have to be considered as well, other structural trends as a function of electron concentration are observed. For example, in the system $MgCu_{2-x}Zn_x$ the sequence of primary Laves phase structure types $MgCu_2 \rightarrow MgNi_2 \rightarrow MgZn_2$ is observed for increasing x, i.e., increasing electron concentration, which is reversed to the trend found for pure main group Laves phase systems.[6,8]

Acknowledgment. This work was supported by the Swedish Research Council (VR). Additionally, we acknowledge funding from the European Community through its "Access to Research Infrastructure Action of the Improving Human Potential Program". We thank Steve Hull at the ISIS Facility, Rutherford Appleton Laboratory, Chilton, U.K., for his assistence in performing the neutron diffraction experiments and Per-Erik Werner at Stockholm University, Stockholm, Sweden, for his help with the refinement of the neutron powder diffraction data.

Supporting Information Available: Four X-ray crystallographic files (in CIF format), a table containing detailed data on the neutron powder refinement, a table containing the interatomic distances A−B in the Laves phases $CaAl_{2-x}Mg_x$, and a figure displaying calculated densities of states of $CaAl_{2-x}Mg_x$. This material is available free of charge via the Internet at http://pubs.acs.org.

IC020596M